ACS APPLIED NANO MATERIALS

www.acsanm.org Article

Aerosol Jet Printing of Phase-Inversion Graphene Inks for High-Aspect-Ratio Printed Electronics and Sensors

Livio Gamba, Santiago Diaz-Arauzo, Mark C. Hersam, and Ethan B. Secor*

Cite This: *ACS Appl. Nano Mater.* 2023, 6, 21133−21140 Read Online

ACCESS | Metrics & More | Article Recommendations | Supporting Information

ABSTRACT: Aerosol jet printing is a technology particularly suited for additive manufacturing of functional microstructures, offering resolutions as high as 10 μm, broad compatibility for electronic nanomaterials, and noncontact deposition, making it compelling for device prototyping and conformal printing. To adapt this method from thin film patterns to taller features, both ink rheology and drying kinetics require careful engineering. Printing in a solvent-rich, low-viscosity state commonly results in a puddle, with liquid-phase spreading and susceptibility to instabilities, whereas printing solvent-depleted aerosol results in a granular morphology with high overspray. Here, we demonstrate a strategy to mitigate this trade-off by tailoring the evolution of ink rheology during the process, using a graphene ink containing the nonsolvent glycerol as an exemplar. During droplet transport to the nozzle, evaporation of volatile primary solvents increases the glycerol concentration, resulting in gel formation. This switch in the ink rheology between the cartridge and substrate maintains the print resolution at high deposition rates. Moreover, multiple layers can be printed in rapid succession to build up high aspect ratio microstructures, as demonstrated by continuously printed cylindrical pillars with diameters on the order of ∼100 μm and aspect ratios as high as ∼10. Finally, the efficacy of this ink formulation strategy for a CuO nanoparticle ink confirms the generalizability of this strategy for a broader scope of colloidal nanomaterial inks. In addition to its utility for microscale additive manufacturing of 2.5D structures, this strategy provides insights into higher deposition rate patterning to improve scalability and throughput of aerosol jet printing.

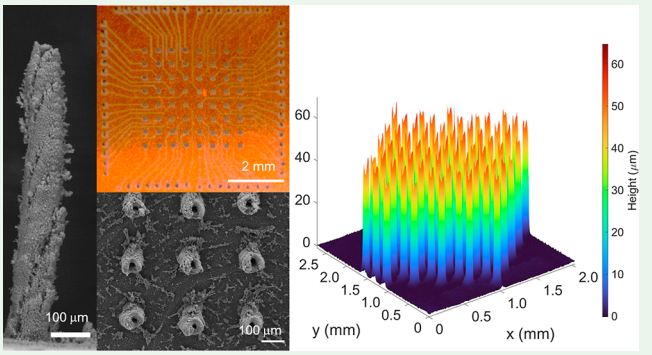

KEYWORDS: *printed electronics, 2.5D additive manufacturing, nanomaterial inks, advanced manufacturing, hybrid electronics*

INTRODUCTION

Digital printing technologies offer a compelling platform for manufacturing electronic devices and systems, offering advantages in design complexity and prototyping agility compared to traditional manufacturing methods.[1] While the field of printed electronics has advanced rapidly, most efforts to date remain focused on thin film structures. Adapting these materials and patterning technologies to more complex 2.5D and 3D microstructures is an emerging area of interest, which can offer design capabilities not possible by using conventional deposition methods. For example, high aspect ratio structures can improve the surface area for electrochemical devices such as sensors and batteries,[2,3] alter fluid−surface interactions to engineer wetting properties,[4] provide routes to complex electronic packaging,[5,6] enable more sophisticated biointegrated electronics,[7] and support modulation of acoustic wave propagation.[8]

Aerosol jet printing (AJP) is a compelling platform to address these opportunities, offering noncontact and digital patterning with high spatial resolution and broad materials compatibility, particularly for colloidal nanomaterials. Due to these advantages over alternative printing methods such as inkjet and screen printing, AJP has enabled frontier work in the area of 2.5D/3D additive electronics, in which 2.5D implies a high aspect ratio for an extruded 2D pattern (i.e., an equivalent 2D design for each horizontal slice).[9,10] In AJP, a liquid ink containing functional materials is atomized to create micron-scale droplets, which are transported to the printhead using a gas flow.[11,12] Within the printhead, a second gas flow surrounds the aerosol stream, focusing the ink droplets through a deposition nozzle onto a surface. The high-velocity jet allows printing with a high standoff distance, a unique advantage required for conformal printing and deposition on nonuniform surface topography.[13,14] However, the rheology requirements for AJP pose a challenge for high aspect ratio patterning. In particular, low viscosity and

Received: September 4, 2023
Revised: October 20, 2023
Accepted: October 26, 2023
Published: November 9, 2023

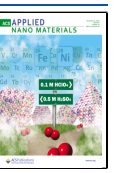

https://doi.org/10.1021/acsanm.3c04207
ACS Appl. Nano Mater. 2023, 6, 21133−21140

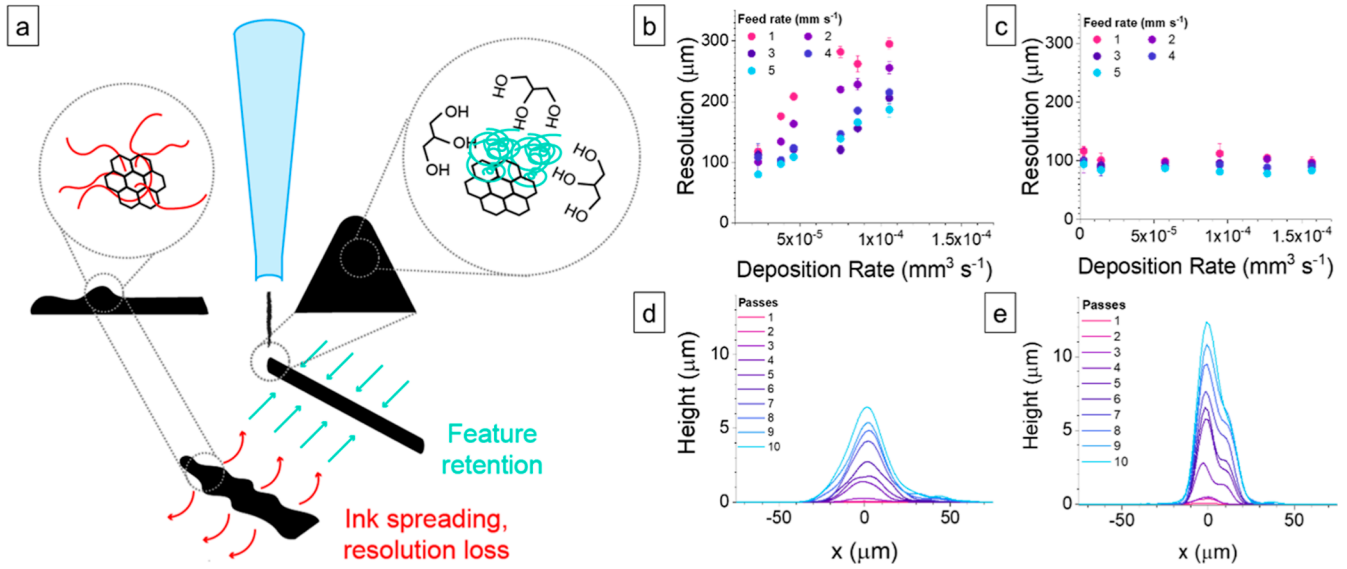

Figure 1. Controlled experiment showing the effect of glycerol addition in the graphene ink. (a) Schematic showing the qualitative effect of glycerol on the reduction of liquid-phase ink spreading following deposition by inducing phase inversion with the polymer dispersant. (b,c) Resolution from optical microscopy plotted as a function of deposition rate for the gly-free and quaternary inks, respectively. (d,e) Profiles of printed multilayer lines for the gly-free and quaternary inks after thermal treatment, respectively.

high fluidity are required for ultrasonic atomization to generate aerosol droplets, but these characteristics lead to liquid-phase spreading and instability following deposition on the surface.[15,16] These issues are exacerbated at the high deposition rates necessary for patterning tall features efficiently. As a result, the ink composition should undergo a change between the cartridge and surface. For certain dielectric inks, UV curing to induce photopolymerization offers one route to achieve this;[5,6] for colloidal inks, it is common to accelerate drying during the process by either formulating the ink with volatile solvents or operating the printer at high temperature,[9,10] which can increase overspray, lead to process sensitivity, and reduce transfer efficiency.

We present an alternative strategy for high-aspect-ratio AJP of colloidal nanomaterials, using graphene as an exemplar material, in which the engineering of the ink composition promotes material gelation between atomization in the cartridge and impaction with the substrate by adding glycerol, a low-volatility nonsolvent for the graphene/polymer composition as previously demonstrated.[17] As the droplets move through the printhead, drying induced by the sheath gas increases the glycerol concentration within the ink droplets.[18] The resulting phase inversion drives gelation of the polymer and dispersed nanomaterials, culminating in suitable rheology for printing at high deposition rates and fabricating multilayer structures without compromising spatial resolution. Where a typical ink forms a puddle, this nonsolvent-containing ink forms a high aspect ratio pillar structure, even for a graphene ink containing less than 1% v/v graphene. This allows versatile patterning of 2.5D pillar structures with digital control to individually alter the placement, height, and other characteristics of each pillar. This is a compelling capability for more advanced biosensors, similar to impressive recent results for neural interfaces and rapid disease detection.[2,19] Moreover, this phase inversion ink strategy is shown to translate to metal oxide nanoparticles, demonstrating the generalizability of the method for 2.5D AJP in a variety of applications.

MATERIALS AND METHODS

Materials and Ink Preparation. Diglyme, Cyrene (dihydrolevoglucosenone), isobutyl acetate, and copper(II) oxide nanoparticles (80 nm) were purchased from Millipore Sigma (St Louis, MO, USA). Nitrocellulose was purchased from Scientific Polymer Products (Ontario, NY), and glycerol was purchased from Fisher Scientific (Waltham, MA). No purification process was performed on any of the purchased chemicals. The graphene powders used in the manufacturing of 2.5D microstructures are prepared with ethyl cellulose following a shear mixing procedure described in detail elsewhere.[18,20] These powders were used to prepare 10 mg mL^{-1} graphene/EC-based inks in conjunction with 5 mg mL^{-1} of nitrocellulose and a solvent mixture containing 40% vol each of isobutyl acetate and diglyme, with the remaining 20% vol consisting of a 1:0, 3:1, or 1:1 mixture (v/v) of Cyrene and glycerol. All components were loaded into 20 mL scintillation vials and agitated for 16 h in an ultrasonic bath to mix the ink prior to printing experiments.

Instrumentation, Characterization Methods, and Image Analysis. A custom-built AJP system was used for all experiments, using a 200 μm tapered plastic nozzle tip (Nordson, Westlake, OH, USA) with a print bed heated to 60 °C. Postprocessing annealing was performed in air using a Lindberg Blue M muffle furnace (Thermo Fisher Scientific, Waltham, MA, USA) with the following procedure: ramp from 25 to 70 °C using a 2 °C min^{-1} heating rate, dwell at 70 °C for 15 min to evaporate residual solvents, ramp to 325 °C with a 2 °C min^{-1} heating rate, dwell for 60 min at 325 °C to decompose dispersants and additives, followed by natural cooling to room temperature. Surface morphology was measured with a Zygo NewView 9000 optical surface profiler (Zygo, Middlefield, CT, USA) with the resulting data being sequentially processed with Gwyddion and MATLAB. Morphological characterization of the printed structures also included scanning electron microscopy (SEM), which was performed with a FEI Quanta 250 FE-SEM (FEI Company, Hillsboro, OR, US). Single-pass line resolution was measured with an optical microscope (Motic, Schertz, TX, USA) operated in dark mode, with the resulting images analyzed using MATLAB.

RESULTS AND DISCUSSION

In this work, ink formulation principles and AJP physics are synergistically applied toward consistent fabrication of high aspect ratio 2.5D graphene microstructures. First, a method-

https://doi.org/10.1021/acsanm.3c04207
ACS Appl. Nano Mater. 2023, 6, 21133−21140

ology to quantitatively assess the trade-off between deposition rate and spatial resolution for a given ink is developed to guide formulation of an ink less susceptible to liquid-phase spreading at high deposition rates. Then, continuous printing of high aspect ratio pillars is pursued to extend the formulation suitability for 2.5D printing. Finally, the versatility of this method is highlighted by demonstrating multimaterial patterns, variable-height pillar arrays, isolated microelectrode arrays, and extension to a metal oxide nanoparticle ink.

Overcoming the Deposition Rate/Resolution Trade-Off in AJP. A key challenge of AJP is the trade-off in spatial resolution and deposition rate. For production environments, a higher deposition rate is typically desired to improve throughput, but excessive deposition of liquid ink in a given region results in liquid-phase spreading that reduces spatial resolution (defined here as the width of a line in the *xy* plane resulting from a single printing pass).[15] One approach to address this challenge is to print in a "dry" or solvent-depleted state, but the corresponding reduction in droplet size is expected to exacerbate overspray and reduce transfer efficiency under these conditions.[21] An alternative approach, in principle, is to reduce the flowability of the ink following deposition, as schematically shown in Figure 1a. However, this strategy presents a challenge for ink formulation, because low viscosity (<10 mPa·s) within the cartridge is a requirement for ultrasonic atomization. To evaluate whether strategic ink engineering can overcome this fundamental drawback, two different inks formulated with graphene/ethyl cellulose powders are used for a preliminary experiment. A control ink, referred to as gly-free ink, is formulated using 40 vol % each of diglyme and isobutyl acetate, with the remaining 20 vol % being Cyrene; a second ink, referred to hereafter as the quaternary ink, is formulated with 10 vol % of Cyrene replaced with glycerol, a low-molecular-weight, high-viscosity liquid that has been shown in previous works to act as a nonsolvent for these powders.[18] The nonsolvent properties of glycerol are exploited to induce coiling of the ethyl cellulose polymer chains, which leads to more efficient atomization,[18] and to promote polymer phase inversion during the advanced stages of drying.[17] Using these two inks, printing experiments spanning a range of carrier gas flow rates are performed to vary the deposition rate. Resolution analyses performed after curing of the printed traces show that features obtained with the gly-free ink exhibit high sensitivity to process parameters, as lines printed at the lowest deposition rate and highest feed rates exhibit the largest line width (Figure 1b). As the deposition rate increases, the resolution becomes worse (i.e., the width of the line increases), as more material is deposited in a single printing pass and spreads on the substrate surface while drying.[22,23] Similar experiments performed with the quaternary ink reveal that line resolution shows less dependence on deposition rate as well as being more invariant with print speed (Figure 1c). Specifically, there is a ~38 μm difference between the most and least resolved features deposited with the quaternary ink, whereas similar measurements on lines printed with the gly-free ink exhibit a resolution range of over ~215 μm. The ability of glycerol to prevent spreading during drying is attributed to its nonsolvent nature, which effectively gels the printed traces in place. This is supported by theoretical estimates of the solvent activity coefficient for Cyrene and glycerol based on UNIFAC calculations (Figure S1).[24,25] In binary mixtures of solvent and polymer (EC or NC), glycerol exhibits a sharp increase in activity coefficient in the polymer-enriched mixture, implying poor solubility and a thermodynamic drive for phase separation, as solubility is inversely related to activity coefficient.[26] Because glycerol has a lower vapor pressure than Cyrene and the primary ink solvents, during drying in either the aerosol phase or following deposition on the surface, the enrichment of glycerol gives rise to phase inversion.[17] Thus, it is the combination of volatility and chemical thermodynamics that makes glycerol particularly suited for this purpose,[27] providing a useful guide for solvent selection to generalize this concept beyond this particular material system. Another phenomenon that could contribute to the enhanced resolution in printed features using the quaternary ink can be found in the inverse Marangoni effect that arises in the late stages of drying. At this point, the solvent composition of the printed trace can be considered to be composed of low levels of isobutyl acetate and diglyme and high percentages of Cyrene and glycerol. If the two solvents with relatively high vapor pressures are neglected, the Marangoni theory predicts a contraction during evaporation for a mixture in which the less volatile component, glycerol (Table S1), also has a lower surface tension than the more volatile solvent,[22] effectively preventing material spreading and improving resolution in the printed line.

Additionally, the fine resolution maintained at high deposition rates for the quaternary ink indicates that the printed traces have a profile taller than that printed without glycerol. To extend this analysis beyond single-pass printed lines, further experiments with multiple printing passes were performed with the intent to determine whether glycerol inclusion can prevent structural collapse of a high aspect ratio feature without compromising resolution. Experiments performed with both gly-free and quaternary inks (Figure 1c,d, respectively) show that the averaged line profile for tall features printed with the gly-free formulation possesses a lower overall resolution of ~100 μm and lower heights (Figure 1c), whereas the quaternary ink produces high-aspect-ratio features roughly twice as tall with a resolution of ~60 μm (Figure 1d). The absence of a complete collapse of features fabricated with the gly-free ink formulation can be attributed to the toolpath used for these experiments (Figure S2), in which lines are allowed to partially dry for 6 to 28 s between each subsequent printing pass. These results establish a strong foundation to target continuous printing of higher aspect ratio structures with minimal consideration of drying between printing passes.

Transition to 2.5D Manufacturing. Leveraging the glycerol-induced gelation of printed lines, we attempted the fabrication of 2.5D structures by printing graphene in a circular pattern. For these experiments, a carrier gas flow rate of 10 sccm, a focusing ratio of 4, and a feed rate of 1 mm s^{-1} were used to create a pillar microstructure, as schematically shown in Figure 2a. The gelation of the printed features induced by glycerol allows continuous deposition of material, improving process efficiency compared to strategies based on layer-by-layer printing which involve frequent interruption via shuttering to balance the rate of material deposition with solvent evaporation.[28] Following printing, the resulting samples are postprocessed in a muffle furnace in air at a temperature of 325 °C to completely remove additives, dispersants, and residual solvents. SEM images reveal the effect that postprocessing conditions have on the qualitative appearance of the final 2.5D microstructure, with a 5 °C min^{-1} heating rate leading to partial pillar collapse but a 2 °C min^{-1} heating rate maintaining the original shape, as demonstrated in Figure 2b for micropillars printed with 40 passes. Although similar microstructures have been previously fabricated using a commercial silver ink,[28] the

https://doi.org/10.1021/acsanm.3c04207
ACS Appl. Nano Mater. 2023, 6, 21133−21140

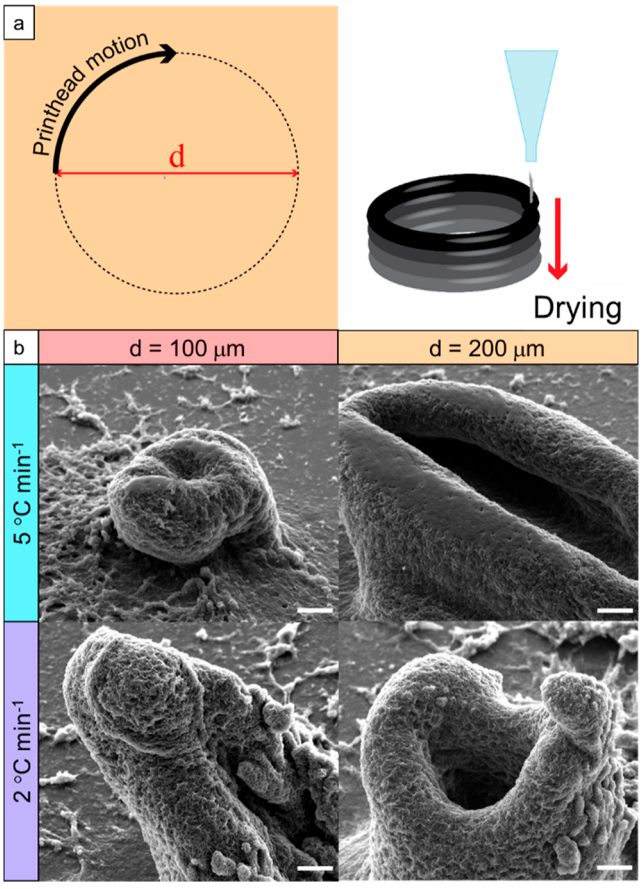

Figure 2. (a) Operational schematic showing additive manufacturing of carbon-based pillar structures. (b) SEM images of 2.5D pillar structures with different diameters, 100 and 200 μm, and postprocessed with different heating rates, 2 and 5 °C min^{-1}. All samples were printed on a silicon chip and fabricated using the quaternary formulation to leverage the glycerol-induced gelation of the deposited material. Scale bars are 20 μm for all SEM images.

structures fabricated in this work do not exclusively rely on strict control over the printing process but also consider the chemistry, thermodynamics, and mechanics of the ink upon deposition, thus illustrating an alternative approach that can be leveraged for manufacturing complex microstructures with different material composition and patterning requirements.

As these results define the experimental conditions for 2.5D manufacturing of graphene micropillars, further samples were printed to vary the lateral density of carbon nanopillars and to understand the size reduction induced by thermal annealing. First, optical profilometry experiments show that a reasonable distance between the outer edges of adjacent pillars that allows for the two structures to be individually defined is 75 μm, but all of the samples shown in this work have a 100 μm lateral spacing. Second, the effects of thermal annealing were also observed with optical profilometry, as shown in Figure S3, with a height reduction of ∼50% after annealing coupled with a significant reduction in the imaged diameter. For completeness, a sample with the same lateral distribution of micropillars was also manufactured using the glycerol-free ink and an intermediate ink containing 5% glycerol and 15% Cyrene. All three samples were annealed using the same procedure and analyzed with optical profilometry (Figure S4). The resulting data reveal that the lack of glycerol does lead to structural distortions even when the slower heating rate of 2 °C min^{-1} is used, with adjacent structures collapsing on each other and thus losing their individual definition. The inclusion of glycerol promotes structural integrity and the retention of micropillar separation during the entire process. A statistical comparison of the three ink formulations validates the improvement observed for the glycerol-containing inks (Figure S5 and Table S2). While both inks containing glycerol achieve an aspect ratio >1.5, the ink containing 10% glycerol exhibits reduced variability and is used for further studies. The gly-free ink achieves an aspect ratio approaching 0.9, but the instability of the pillars on the surface is a clear barrier to reliable fabrication.

Once the conditions to consistently fabricate 2.5D structures with AJP were determined, an array of micropillars was integrated into a planar electrode. Decreasing the carrier gas flow rate to 8 sccm allowed printing of hollow cylindrical structures that withstand postprocessing and handling without sacrificing structural integrity, as shown by both optical profilometry and SEM (Figure 3). Here, an array of graphene micropillars is fabricated in a grid, showing consistent geometry with pillars printed one at a time rather than layer by layer. While some large aggregations of graphene are observed across the surface of the planar electrode, these align with the circular toolpath of the planar electrode rather than being localized near the pillars themselves. There is some additional material surrounding the base of each pillar, but this exhibits a morphology distinct from dry overspray, which is an aerosol-phase phenomenon. Rather, this material is attributed to liquid-phase effects aligned with phase inversion.

The optical profilometry data (Figure 3a) reveal micropillars printed with 40 layers, with a maximum height of 54.2 ± 2.6 μm (n = 59 pillars in image, Table S3). A slight variation in height around the rim of each pillar is attributed to the motion system for printing, which has finite acceleration. In printing a few layers, this is imperceptible, but when repeated over many passes, the slight decrease in speed at the sides of the pillar leads to a small increase in height.

This initial demonstration of a large pillar array confirms the suitability of the phase inversion ink for printing high aspect ratio structures. Allowing continuous printing of pillars without relying on heat transport from the substrate to balance deposition and drying simplifies process design and supports extension to even taller structures. To validate this, 2.5D structures with a nominal diameter of 100 μm were printed with 50−300 layers to determine what limits the achievable height. This efficient printing process is shown in Video S1, and SEM images of pillars with 50−300 layers are shown in Figure 4. Under these printing conditions, the structures exhibited a base diameter of ∼105 μm and aspect ratios of ∼2.4, 4.3, 7.5, and 10.5 for 50, 100, 150, and 200 layers, respectively. Notably, the pillar with 300 printed layers exhibits a wider diameter of ∼160 μm, resulting in a lower aspect ratio of ∼6.6 and implying a limit to aspect ratio within these printing/drying/curing conditions. In similar tests with a slower heating rate (1 °C min^{-1}), the structures have lower height overall but a more consistent increase in height with additional layers for prints up to 500 layers, suggesting more densification during curing and better mechanical stability (Figure S6, Table S4).

Leveraging Design Freedom of Advanced Manufacturing. To extend the printing evaluation to more complex fabrication constraints, three additional criteria were considered: process integration with additional inks, nonuniform pillar heights, and isolated pillar electrodes. These are selected to highlight the broad design freedom afforded by this additive

https://doi.org/10.1021/acsanm.3c04207
ACS Appl. Nano Mater. 2023, 6, 21133−21140

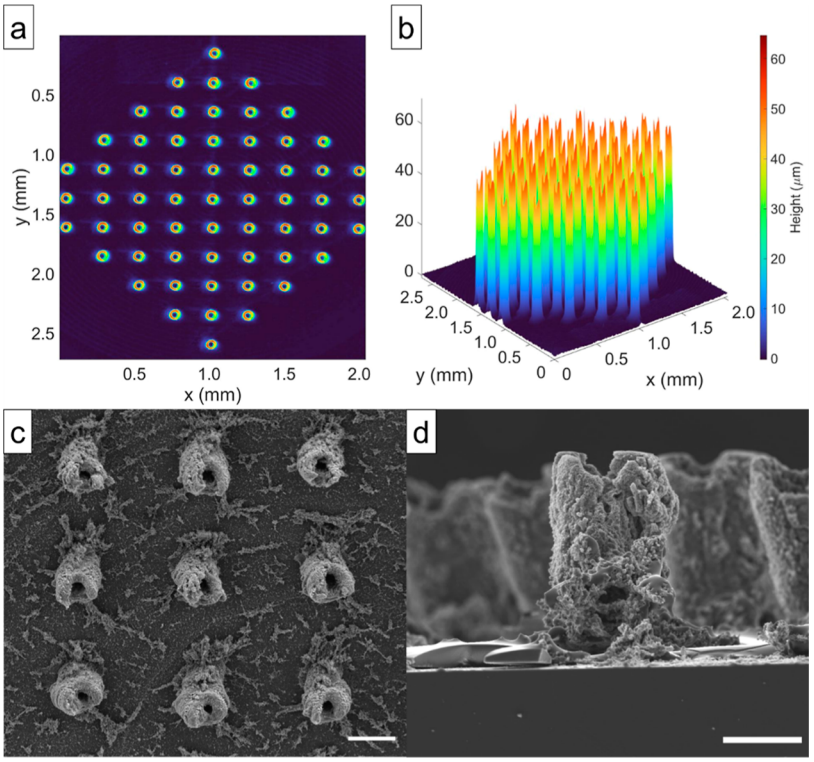

Figure 3. (a) Top view optical profilometry image of a 2.5D pillar structure array integrated onto a planar electrode and (b) its corresponding surface plot. (c) Top-down SEM photograph of a graphene sample with 2.5D pillar structures, scale bar 100 μm, and (d) its corresponding cross-sectional image, scale bar 50 μm. Both samples were printed on Kapton.

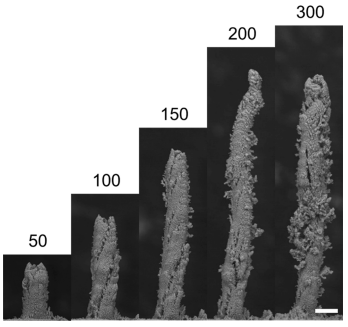

Figure 4. SEM images of micropillars printed with increasing passes (50−300 as indicated) and annealed with a 2 °C min^{-1} heating rate; scale bar: 100 μm.

patterning method. First, a dielectric layer of PMMA was deposited in the spacing between the pillars of an annealed pillar array, as shown in Figure 5a,b. The characteristic high resolutions achievable with AJP are leveraged here to deposit the dielectric around the base of each pillar. Micropillars of silver were recently demonstrated by AJP, with subsequent functionality to support COVID detection in ∼10 s,[2] a remarkable advance for rapid disease diagnosis. Using a dielectric layer to passivate the planar base of the electrode array, in this context, can prevent nonspecific binding during analyte detection to reduce noise and improve sensitivity.[29] On the surface of this device, the retention of the hollow graphene micropillars validates the precise deposition of PMMA around the 2.5D structures, which would consequently allow for chemical functionalization only on the pillar sides. Moreover, the pillars remain stable to the high-velocity gas jet during PMMA fabrication, confirming their suitability to withstand the mechanical environment of subsequent processing steps. It is worth noting the cracks observed in the dielectric layer in Figure 5b are introduced during the cleaving of the sample necessary for imaging and are not representative of the as-fabricated sample morphology (as shown in Figure 5a).

The design freedom available with direct write methodologies was also exploited to introduce pillars with specific spatial distribution (Figure 5c) or height (Figure 5d) with the intent to demonstrate the possibility of device manufacturing with custom surface properties, for potential applications in the field of microfluidics.[30] In particular, a uniform array of pillars exhibits a high contact angle with water due to a Cassie−Baxter state (Figure S7). By introducing regions devoid of pillars (Figure 5c) or with variations in pillar height (Figure 5d), the behavior of water droplets can be manipulated (Video S2). Here, the use of graphene rather than traditional polymer or metal oxide materials to create a Cassie−Baxter surface provides opportunities for exploiting the electrical, thermal, optical, and other functionalities of graphene. Moreover, the ability to vary pillar height across a sample, without introducing additional fabrication steps, highlights the utility of additive methods for micropillar array fabrication.

Inspired by previous studies introducing graphene-based neural devices,[31] the ability to customize devices by leveraging the properties of additive manufacturing was further expanded upon by fabricating microelectrode arrays which included 2.5D structures with specific spatial distribution and pillar height, as shown in Figure 6. Panat et al. recently demonstrated the application of a printed microelectrode array (MEA) for brain monitoring, in which AJP micropillars allowed a high-resolution neural interface with design freedom to support multiple planes of sensing.[19] In this demonstration, a plasma-focused ion beam

https://doi.org/10.1021/acsanm.3c04207
ACS Appl. Nano Mater. 2023, 6, 21133−21140

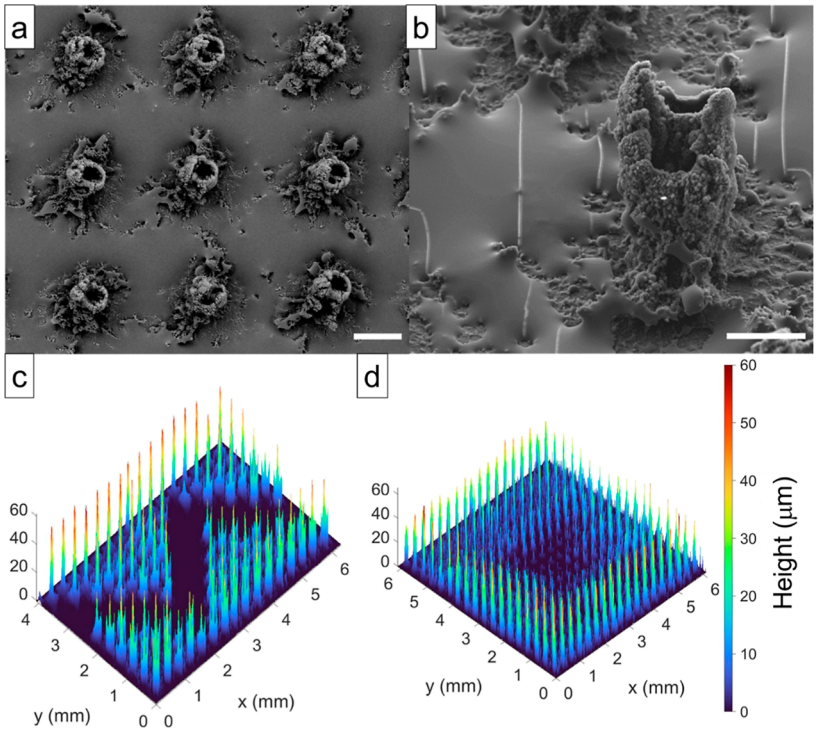

Figure 5. (a) Top-down and (b) tilted (~30°) views of an electrode printed on silicon to include 2.5D carbon microstructures as well as a dielectric layer of PMMA deposited between pillars, with 100 and 50 μm scale bars, respectively. (c) Graphene sample printed on Kapton containing a pillar-free region to direct fluid wetting and (d) 2.5D sample printed on Kapton programmed to have nonuniform pillar height, with a depression toward the center of the specimen.

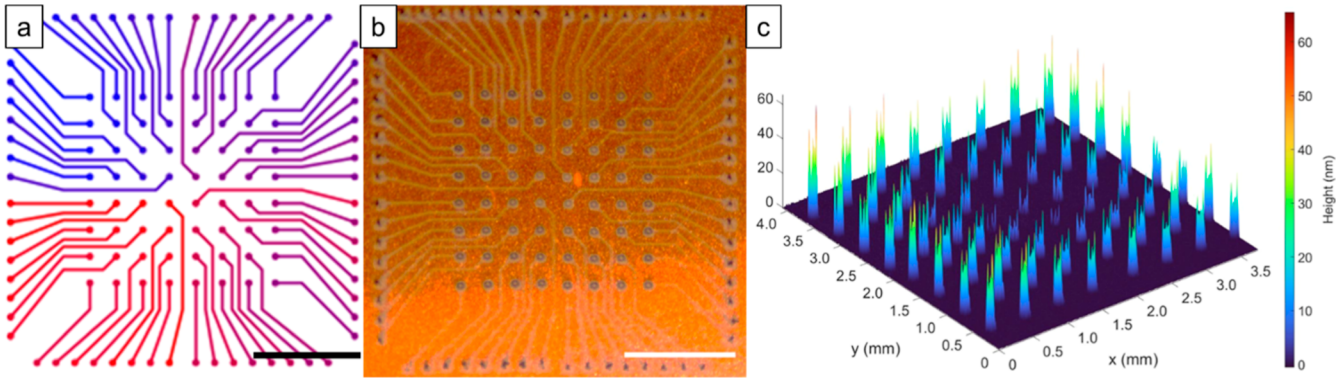

Figure 6. (a) Toolpath used for the manufacturing of the electrode array, (b) the respective processed graphene sample printed on Kapton, and (c) its surface profile. Scale bar 2 mm for (a,b).

processing step was required to remove overspray to electrically isolate micropillars, adding processing time and an appreciable cost. Here, a 64-electrode array was printed in which the innermost electrodes had the smallest height, which would correspond to different planes of neurons targeted for interrogation. Because this ink formulation allows a high aspect ratio even when printing in a wet state, reduced overspray between pillars is evident (Figure S8), supporting an efficient process flow. This is significant when each electrode must be electronically isolated, providing a platform for interrogating or manipulating electrochemistry or electrophysiological signals. Moreover, the high design freedom afforded by digital fabrication methodologies could be a distinguishing capability for more sophisticated bioelectronic interfaces, such as shell MEAs for organoids.[32]

Generalization to Alternative Functional Materials. The results thus far demonstrate a broad degree of manufacturing versatility for a graphene ink by engineering the ink rheology. To validate that this concept can translate to additional materials, a metal oxide nanoparticle ink was prepared with a similar formulation. Copper(II) oxide nanoparticles were dispersed in the same solvent mixture with ethyl cellulose and nitrocellulose as dispersants. Following the same experimental procedures as for graphene, this ink allowed fabrication of 2.5D ceramic structures, which maintained their morphology after being cured at 325 °C (Figure S9). This reveals the possibility of generalizing this strategy to a wider range of metal oxides, which could provide diverse electrochemical functionality, among other properties, and streamline development of composite inks containing graphene and metal oxide nanoparticles.

https://doi.org/10.1021/acsanm.3c04207
ACS Appl. Nano Mater. 2023, 6, 21133−21140

Outside of its relevance for fabricating high aspect ratio structures, the early results of this study emphasize the importance of these rheology considerations for ameliorating the trade-off between spatial resolution and deposition rate during AJP. Gelation of colloidal dispersions is a well-studied phenomenon, and it is likely that this mechanism is relevant to current inks, whether or not its use is deliberate. More explicitly, recognizing this as an opportunity to engineer print characteristics and designing both the formulation and processing parameters to better exploit it can offer broad value to streamline ink and process development for both 2D and 2.5D AJP.

CONCLUSIONS

In this work, the fabrication of microscale 2.5D graphene structures using AJP was demonstrated by holistically considering both the process parameters of the additive manufacturing technique and the chemical effects of the ink formulation. In this specific case, the inclusion of a high-viscosity, low-molecular-weight compound, glycerol, mitigates the lateral spreading of deposited ink to support high aspect ratio features as a result of a rheology transition during printing. Coupling AJP process engineering fundamentals with ink formulation principles also allowed for the deposition of 2.5D structures without interrupting the printing process to allow drying, supporting a reduction in manufacturing time. Lastly, the viscosity effects induced by the presence of glycerol in printed traces were demonstrated for a carbon nanomaterial, graphene, as well as for an ink containing copper(II) oxide nanoparticles formulated with the same solvent and dispersant system. Alongside the impact of printing typical circuit features (i.e., interconnects and electrodes) with higher deposition rate and precision, micropillars with aspect ratios as high as ∼10 were demonstrated. These results highlight how general ink formulation concepts can be successfully applied to a wider range of nanomaterials, which can guide ink development efforts tailored to specific processing requirements and offer great potential for widespread application, such as in electrochemical sensing, microfluidics, and surface engineering.

ASSOCIATED CONTENT

Supporting Information

The Supporting Information is available free of charge at https://pubs.acs.org/doi/10.1021/acsanm.3c04207.

Solvent properties, print pattern details, additional characterization of gly-free and quaternary ink deposition, additional characterization of printed graphene structures, and characterization of printed CuO structures (PDF)

Video showing the efficient printing process of depositing 2.5D structures (MP4)

Video showing the behavior of water droplets on printed structures (MP4)

AUTHOR INFORMATION

Corresponding Author

Ethan B. Secor − *Department of Mechanical Engineering, Iowa State University, Ames, Iowa 50010, United States;* orcid.org/0000-0003-2324-1686; Email: esecor@iastate.edu

Authors

Livio Gamba − *Department of Mechanical Engineering, Iowa State University, Ames, Iowa 50010, United States*

Santiago Diaz-Arauzo − *Department of Materials Science and Engineering, Northwestern University, Evanston, Illinois 60208, United States*

Mark C. Hersam − *Department of Materials Science and Engineering, Northwestern University, Evanston, Illinois 60208, United States; Department of Chemistry and Department of Electrical and Computer Engineering, Northwestern University, Evanston, Illinois 60208, United States;* orcid.org/0000-0003-4120-1426

Complete contact information is available at: https://pubs.acs.org/10.1021/acsanm.3c04207

Author Contributions

The manuscript was written through contributions of all authors. All authors have given approval to the final version of the manuscript.

Notes

The authors declare no competing financial interest.

ACKNOWLEDGMENTS

L.G. and E.B.S. gratefully acknowledge funding support from the National Science Foundation under NSF CMMI-2224303. E.B.S. further acknowledges the Department of Mechanical Engineering at Iowa State University for access to characterization facilities, along with support from the 3M Non-Tenured Faculty Award program. S.D.-A. and M.C.H. acknowledge support from the National Science Foundation MADE-PUBLIC Future Manufacturing Research Grant Program (NSF award number CMMI-2037026).

ABBREVIATIONS

AJP, aerosol jet printing; 2.5D, 2.5 dimensional; 3D, 3-dimensional

REFERENCES

(1) Wilkinson, N. J.; Smith, M. A. A.; Kay, R. W.; Harris, R. A. A Review of Aerosol Jet Printing—a Non-Traditional Hybrid Process for Micro-Manufacturing. *Int. J. Adv. Manuf. Technol.* **2019**, *105* (11), 4599−4619.

(2) Ali, M. A.; Hu, C.; Jahan, S.; Yuan, B.; Saleh, M. S.; Ju, E.; Gao, S. J.; Panat, R. Sensing of COVID-19 Antibodies in Seconds via Aerosol Jet Nanoprinted Reduced-Graphene-Oxide-Coated 3D Electrodes. *Adv. Mater.* **2021**, *33* (7), No. e22006647.

(3) Saleh, M. S.; Li, J.; Park, J.; Panat, R. 3D Printed Hierarchically-Porous Microlattice Electrode Materials for Exceptionally High Specific Capacity and Areal Capacity Lithium Ion Batteries. *Addit. Manuf.* **2018**, *23*, 70−78.

(4) Jafari, R.; Cloutier, C.; Allahdini, A.; Momen, G. Recent Progress and Challenges with 3D Printing of Patterned Hydrophobic and Superhydrophobic Surfaces. *Int. J. Adv. Manuf. Technol.* **2019**, *103* (1−4), 1225−1238.

(5) Gu, Y.; Hines, D. R.; Yun, V.; Antoniak, M.; Das, S. Aerosol-Jet Printed Fillets for Well-Formed Electrical Connections between Different Leveled Surfaces. *Adv. Mater. Technol.* **2017**, *2* (11), 1700178.

(6) Rahman, T.; Renaud, L.; Heo, D.; Renn, M.; Panat, R. Aerosol Based Direct-Write Micro-Additive Fabrication Method for Sub-Mm 3D Metal-Dielectric Structures. *J. Micromech. Microeng.* **2015**, *25* (10), 107002.

(7) Xu, L.; Hu, C.; Huang, Q.; Jin, K.; Zhao, P.; Wang, D.; Hou, W.; Dong, L.; Hu, S.; Ma, H. Trends and Recent Development of the Microelectrode Arrays (MEAs). *Biosens. Bioelectron.* **2021**, *175*, 112854.

(8) Assouar, B.; Liang, B.; Wu, Y.; Li, Y.; Cheng, J.-C.; Jing, Y. Acoustic Metasurfaces. *Nat. Rev. Mater.* **2018**, *3* (12), 460−472.
(9) Saleh, M. S.; Hu, C.; Panat, R. Three-Dimensional Micro-architected Materials and Devices Using Nanoparticle Assembly by Pointwise Spatial Printing. *Sci. Adv.* **2017**, *3*, No. e1601986.
(10) Chen, X.; Lawrence, J. M.; Wey, L. T.; Schertel, L.; Jing, Q.; Vignolini, S.; Howe, C. J.; Kar-Narayan, S.; Zhang, J. Z. 3D-Printed Hierarchical Pillar Array Electrodes for High-Performance Semi-Artificial Photosynthesis. *Nat. Mater.* **2022**, *21* (7), 811−818.
(11) Hines, D. R.; Gu, Y.; Martin, A. A.; Li, P.; Fleischer, J.; Clough-Paez, A.; Stackhouse, G.; Dasgupta, A.; Das, S. Considerations of Aerosol-Jet Printing for the Fabrication of Printed Hybrid Electronic Circuits. *Addit. Manuf.* **2021**, *47*, 102325.
(12) Secor, E. B. Principles of Aerosol Jet Printing. *Flexible Printed Electron.* **2018**, *3*, 035002.
(13) Kaindl, R.; Gupta, T.; Blümel, A.; Pei, S.; Hou, P.-X.; Du, J.; Liu, C.; Patter, P.; Popovic, K.; Dergez, D.; Elibol, K.; Schafler, E.; Liu, J.; Eder, D.; Kieslinger, D.; Ren, W.; Hartmann, P.; Waldhauser, W.; Bayer, B. C. Aerosol Jet Printing of Graphene and Carbon Nanotube Patterns on Realistically Rugged Substrates. *ACS Omega* **2021**, *6* (50), 34301−34313.
(14) Paulsen, J. A.; Renn, M.; Christenson, K.; Plourde, R. Printing Conformal Electronics on 3D Structures with Aerosol Jet Technology. In *2012 Future of Instrumentation International Workshop (FIIW)*, 2012; pp 1−4.
(15) Tafoya, R. R.; Secor, E. B. Understanding Effects of Printhead Geometry in Aerosol Jet Printing. *Flexible Printed Electron.* **2020**, *5*, 035004.
(16) Feng, J. Q. Sessile Drop Deformations under an Impinging Jet. *Theor. Comput. Fluid Dyn.* **2015**, *29* (4), 277−290.
(17) Secor, E. B.; Dos Santos, M. H.; Wallace, S. G.; Bradshaw, N. P.; Hersam, M. C. Tailoring the Porosity and Microstructure of Printed Graphene Electrodes via Polymer Phase Inversion. *J. Phys. Chem. C* **2018**, *122* (25), 13745−13750.
(18) Gamba, L.; Johnson, Z. T.; Atterberg, J.; Diaz-Arauzo, S.; Downing, J. R.; Claussen, J. C.; Hersam, M. C.; Secor, E. B. Systematic Design of a Graphene Ink Formulation for Aerosol Jet Printing. *ACS Appl. Mater. Interfaces* **2023**, *15* (2), 3325−3335.
(19) Saleh, M. S.; Ritchie, S. M.; Nicholas, M. A.; Gordon, H. L.; Hu, C.; Jahan, S.; Yuan, B.; Bezbaruah, R.; Reddy, J. W.; Ahmed, Z.; Chamanzar, M.; Yttri, E. A.; Panat, R. P. CMU Array: A 3D Nanoprinted, Fully Customizable High-Density Microelectrode Array Platform. *Sci. Adv.* **2022**, *8* (40), No. eabj4853.
(20) Secor, E. B.; Prabhumirashi, P. L.; Puntambekar, K.; Geier, M. L.; Hersam, M. C. Inkjet Printing of High Conductivity, Flexible Graphene Patterns. *J. Phys. Chem. Lett.* **2013**, *4*, 1347−1351.
(21) Secor, E. B. Guided Ink and Process Design for Aerosol Jet Printing Based on Annular Drying Effects. *Flexible Printed Electron.* **2018**, *3* (3), 035007.
(22) Wang, Z.; Orejon, D.; Takata, Y.; Sefiane, K. Wetting and Evaporation of Multicomponent Droplets. *Phys. Rep.* **2022**, *960*, 1−37.
(23) Baumgartner, D. A.; Shiri, S.; Sinha, S.; Karpitschka, S.; Cira, N. J. Marangoni Spreading and Contracting Three-Component Droplets on Completely Wetting Surfaces. *Proc. Natl. Acad. Sci. U.S.A.* **2022**, *119* (19), No. e2120432119.
(24) Zhong, C.; Sato, Y.; Masuoka, H.; Chen, X. Improvement of Predictive Accuracy of the UNIFAC Model for Vapor-Liquid Equilibria of Polymer Solutions. *Fluid Phase Equilib.* **1996**, *123* (1−2), 97−106.
(25) DDBST—DDBST GmbH. http://www.ddbst.com/ (accessed Oct 19, 2023).
(26) Hilal, S. H.; Karickhoff, S. W.; Carreira, L. A. Prediction of the Solubility, Activity Coefficient and Liquid/Liquid Partition Coefficient of Organic Compounds. *QSAR Comb. Sci.* **2004**, *23* (9), 709−720.
(27) Blake, A. J.; Kohlmeyer, R. R.; Hardin, J. O.; Carmona, E. A.; Maruyama, B.; Berrigan, J. D.; Huang, H.; Durstock, M. F. 3D Printable Ceramic-Polymer Electrolytes for Flexible High-Performance Li-Ion Batteries with Enhanced Thermal Stability. *Adv. Energy Mater.* **2017**, *7* (14), 1602920.
(28) Ali, M. A.; Hu, C.; Yuan, B.; Jahan, S.; Saleh, M. S.; Guo, Z.; Gellman, A. J.; Panat, R. Breaking the Barrier to Biomolecule Limit-of-Detection via 3D Printed Multi-Length-Scale Graphene-Coated Electrodes. *Nat. Commun.* **2021**, *12* (1), 7077.
(29) Huang, X.-J.; O'Mahony, A. M.; Compton, R. G. Microelectrode Arrays for Electrochemistry: Approaches to Fabrication. *Small* **2009**, *5* (7), 776−788.
(30) Bocanegra Evans, H.; Gorumlu, S.; Aksak, B.; Castillo, L.; Sheng, J. Holographic Microscopy and Microfluidics Platform for Measuring Wall Stress and 3D Flow over Surfaces Textured by Micro-Pillars. *Sci. Rep.* **2016**, *6* (1), 28753.
(31) Park, D.-W.; Schendel, A. A.; Mikael, S.; Brodnick, S. K.; Richner, T. J.; Ness, J. P.; Hayat, M. R.; Atry, F.; Frye, S. T.; Pashaie, R.; Thongpang, S.; Ma, Z.; Williams, J. C. Graphene-Based Carbon-Layered Electrode Array Technology for Neural Imaging and Optogenetic Applications. *Nat. Commun.* **2014**, *5* (1), 5258.
(32) Huang, Q.; Tang, B.; Romero, J. C.; Yang, Y.; Elsayed, S. K.; Pahapale, G.; Lee, T.-J.; Morales Pantoja, I. E.; Han, F.; Berlinicke, C.; Xiang, T.; Solazzo, M.; Hartung, T.; Qin, Z.; Caffo, B. S.; Smirnova, L.; Gracias, D. H. Shell Microelectrode Arrays (MEAs) for Brain Organoids. *Sci. Adv.* **2022**, *8* (33), No. eabq5031.

https://doi.org/10.1021/acsanm.3c04207
ACS Appl. Nano Mater. 2023, 6, 21133−21140